Implementation of B_0 shimming with ferromagnetic ink.

Laura Dupas

M1 PAM Université Paris-Sud 11

Internship at the CEA Saclay / DSV / I2BM / Neurospin / LRMN

Internship supervisor: Christopher Wiggins

June 29, 2012

Acknowledgments

Cette étude a été réalisée au laboratoire LRMN au centre de recherche NeuroSpin du CEA de Saclay, sous la direction de Christopher Wiggins et de Karl Edler que je tiens à remercier pour leur accueil au sein de l'équipe.

Thanks to Karl Edler for his patience when explaining me the principles of spherical harmonics and resolving computer problems and for his advice regarding programming as well.

Pour leur accueil et leurs discussions philosophiques, je remercie Aurélien et les doctorants du 2ème étage.

Contents

List of Figures

Chapter 1

Introduction

NeuroSpin is a research center which belongs to the Life Science Direction of the CEA. It is dedicated to neuroimaging and its aim is to better understand the human brain. The research is focused on development, functional architecture and diseases of the brain and on the improvement of MRI techniques at ultra high magnetic fields (UHF) of 7 Tesla (T) and higher. The greater resolution available with these high field strengths allows neurologists to view very fine structures in the living brain. Currently the NeuroSpin platform has four MRI systems: 7 T and 17.2 T MRI systems for pre-clinical imaging, and 3 T and 7 T MRI systems for clinical research on humans. In 2014 a unique 11.7 T clinical system will be installed. NeuroSpin is composed of five laboratories: LBI and LBIOM (biology and biomedical research), LCogn (cognitive neuroimaging), LNAO (neurocomputing research) and LRMN (methodological research for imaging).

LRMN is the laboratory I worked in, particularly in a team whose research is specialized on overcoming the technical problems of UHF imaging. Since the signal to noise ratio (SNR) rises approximately linearly with the field strength, UHF-MRI allows higher spatial resolution and/or shortens the acquisition time. One of the biggest difficulties of working at UHF is to keep both the static and radiofrequency magnetic fields homogeneous because the presence of irregularly shaped samples and air-tissue interfaces disturbs the magnetic field [2]. To correct heterogeneities in a static applied field, a process called shimming is used by adjusting currents through specially shaped coils (active shimming) or by adding ferromagnetic material (passive shimming). Active shimming is usually limited by the hardware, both in terms of strength (coil and amplifier specifications) and spatial order (the number of supplied shim coils). The subject of my internship is to implement a technique suggested some years ago [3], whereby laser printer toner is used to perform passive shimming. The idea is to measure the field distribution in the magnet, deduce the distribution of toner needed to correct this field and then print the produced distribution of ink on a paper and place it around the antenna. Initially this experiment is done on a spherical sample at 7 T, but once the concept is mastered, it can be extended to primates and then humans and possibly

later to a higher field (17 T). Once this method is implemented, material is readily available so this is a very attractive method. The next step of this study would be to decrease the time needed to calculate and print the individual ink shim pattern to adapt it to every subject examined.

In this study, my job was to improve a python program which calculates the distribution and the amount of ink needed to homogenize the field and to write a postscript program to print the produced matrix. I then tested the printed ink matrix on the 7T MRI system with a phantom to know if the results were correct and the changes significant.

Chapter 2

Nuclear Magnetic Resonance

2.1 Macroscopic magnetization

MRI, meaning Magnetic Resonance Imaging, is based on the phenomenon of Nuclear Magnetic Resonance (NMR). Some nuclei such as hydrogen have a significant magnetic moment due to their net spin:

$$\mu = \gamma \mathbf{S} \tag{2.1}$$

μ : nuclear magnetic moment

S: spin

γ : gyromagnetic ratio in $rad.s^{-1}.T^{-1} = 2.675 * 10^8 rad/s/T$ for hydrogen.

With no applied magnetic field and at equilibrium, each spin in a sample has a random orientation so the total macroscopic magnetization is zero. When a magnetic field $\mathbf{B_0}$ is applied, spins line up along the axis of this field. As protons obey the laws of quantum physics, only two spin orientations are possible: parallel or antiparallel. These orientations correspond to energy levels: $E_{up} = \frac{-\gamma \hbar B_0}{2}$ and $E_{down} = \frac{\gamma \hbar B_0}{2}$. There are more parallel spins than antiparallel ones because the up level has a lower energy, thus the total macroscopic magnetization $\mathbf{M}$ is in the same direction and parallel to $\mathbf{B_0}$. The spin population difference in the two spin states is related to their energy difference, according to Boltzmann relationship [4]:

$$\frac{N_{up}}{N_{down}} = e^{\frac{\Delta E}{K.T}} \tag{2.2}$$

$\Delta E = \gamma \hbar B_0$ is the difference of energy between E_{up} and E_{down}

K : Boltzmann constant $= 1.38 * 10^{-23} J/K$

T: temperature of the spin system

N_{up}: number of pointing-up spins

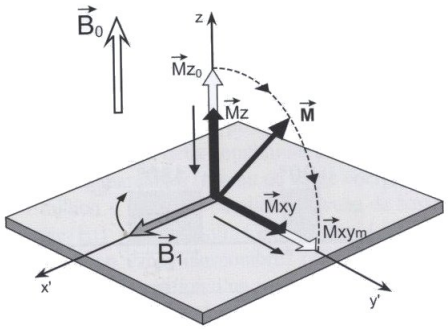

Figure 2.1: $\mathbf{M_z}$ decreases whereas $\mathbf{M_{xy}}$ rises [1]

N_{down}: number of pointing-down spins

ΔE rises linearly with B_0 thus increasing N_{up} and M by the same way. As explained later, M corresponds to the signal therefore when we have a higher magnetic field we observe increased signal [1].

2.2 Oscillating magnetic field $\mathbf{B_1}$

μ precesses around $\mathbf{B_0}$ with an angular frequency $\omega_0 = B_0\gamma$, called the Larmor frequency. At equilibrium, the total macroscopic magnetization $\mathbf{M}$ lines up with $\mathbf{B_0}$ in the z-direction and is referred to as $\mathbf{M_{z0}}$. The magnetization is only observed in the xy-plane (as seen later) so for detection it needs to be brought into this plane. To achieve this an oscillating magnetic field $\mathbf{B_1}$ is added in the xy plane to disturb the equilibrium. The rotation frequency of $\mathbf{B_1}$ has to be the same as Larmor frequency to allow an energy transfer to the spin system. $\mathbf{B_1}$ is a RF field. The radiofrequency (RF) field is created by an oscillating current in a coil called a transmitting antenna. In the rotating frame of $\mathbf{B_0}$, $\mathbf{M}$ precesses at the angular frequency $\omega_1 = \gamma B_1 (= \omega_r)$ around $\mathbf{B_1}$ and is static around $\mathbf{B_0}$. But in the rotating frame of $\mathbf{B_1}$, $\mathbf{M}$ is static around $\mathbf{B_1}$ and precesses around $\mathbf{B_0}$ at ω_0.

When $\mathbf{B_1}$ is applied, $\mathbf{M_z}$ (longitudinal magnetization) decreases whereas $\mathbf{M_{xy}}$ (transversal magnetization) increases thanks to induced coherence of the spins: $\mathbf{M}$ rotates towards the xy plane (figure 2.1). Depending on the power and the duration of RF excitation, $\mathbf{M}$ would rotate by a different angle. If the angle of the excitation is 90 degrees, the entire $\mathbf{M}$ would be on the xy plane. After excitation, $\mathbf{M}$ returns to equilibrium, which implies a decrease of $\mathbf{M_{xy}}$ and a progressive regrowth of $\mathbf{M_z}$. This phenomenon is referred to as relaxation [1].

Free Induction Decay FID.

The reduction of transversal magnetization is quicker than the regrowth of $\mathbf{M_z}$. $\mathbf{M_{xy}}$ describes a spiral in the xy plane (figure 2.2) that induces a magnetic field or radiofrequency wave, called a free induction

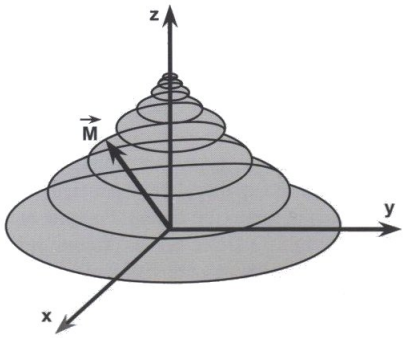

Figure 2.2: $\mathbf{M}$ precesses around $\mathbf{B_0}$ [1]

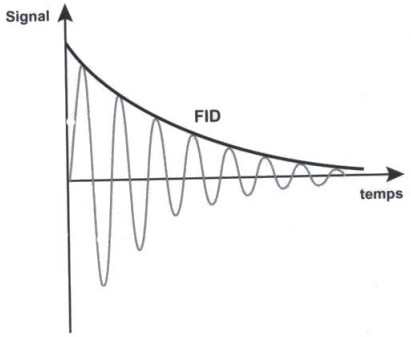

Figure 2.3: Free Induction Decay [1]

decay (FID). It is collected and transformed into a measurable electrical signal by a coil or reception antenna placed around the sample. The decay of $\mathbf{M_{xy}}$ can be represented by a damped sinusoid with an exponential time constant T2 (figure 2.3).

2.3 Relaxation phenomena

Following the excitation, these phenomena would occur [1]:

- The recovery of the longitudinal magnetization $\mathbf{M_z}$ referred to longitudinal relaxation (T1 relaxation).
- The destruction of the transverse magnetization $\mathbf{M_{xy}}$ referred to transverse relaxation (T2 relaxation).

2.3.1 Longitudinal relaxation (T1)

When a 90 degree RF excitation is applied, $\mathbf{M}$ is on the xy plane so $\mathbf{M_z}$ disappears. After the end of RF excitation, the system naturally returns to equilibrium. $\mathbf{M_z}$ regrowth is known as longitudinal relaxation or T1 relaxation due to an exponential increase of $\mathbf{M_z}$ with T1 as characteristic time constant for a given

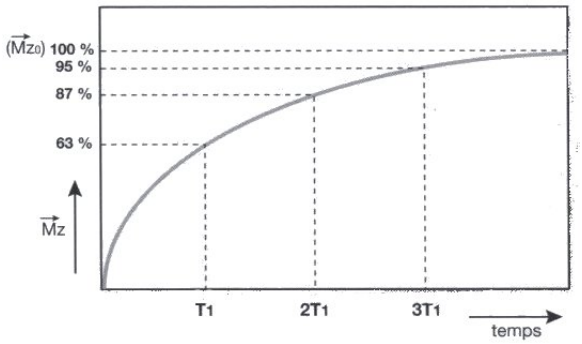

Figure 2.4: Regrowth of $\mathbf{M_z}$: $M_z(t) = M_0(1 - e^{\frac{-t}{T1}})$ [1]

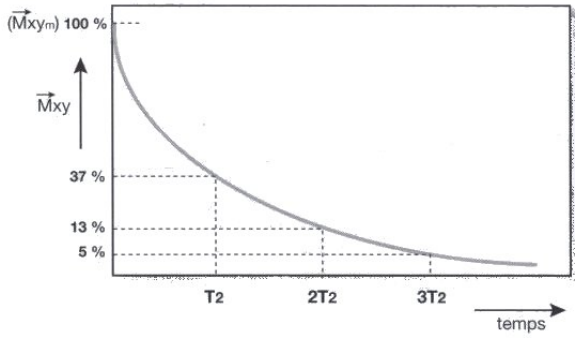

Figure 2.5: Decrease of $\mathbf{M_{xy}}$: $M_{xy}(t) = M_0 e^{\frac{-t}{T2}}$ [1]

sample. T1 corresponds to the time at which 63% of the magnetization has recovered (figure 2.4).

In NMR, each sample has its characteristic T1. In biological tissue, $500ms < T1 < 2000ms$. T1 differences are used to distinguish tissue, indeed MRI parameters can be changed to obtain a T1-weighted image. A particular example is for distinguishing white and grey matter.

2.3.2 Transversal relaxation (T2)

$\mathbf{M_{xy}}$ appears by spin coherence due to a 90 degree RF excitation. At the end of the excitation, a dephasing of the spins occurs and thus $\mathbf{M_{xy}}$ decreases and drops to zero. This is known as transversal relaxation or spin-spin relaxation because this phenomenon is the consequence of interaction between protons. Transversal relaxation is also known as T2 relaxation due to an exponential decrease of $\mathbf{M_{xy}}$ with T2 (ms) as time constant. T2 is a NMR characteristic of the sample (figure 2.5).

For biological tissue: $50ms < T2 < 200ms$. $T2 > T1$ is impossible as T1 means reaching equilibrium so $T2 << T1$. Images are T2-weighted when differences in T2 are used to distinguish tissue.

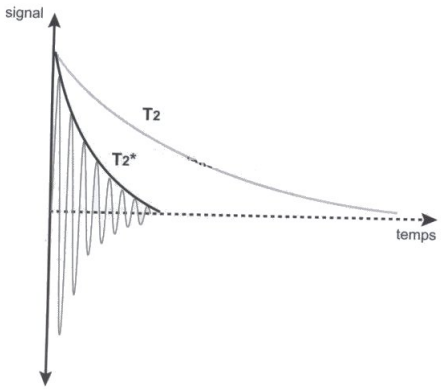

Figure 2.6: Signal: $M_{xy}(t) = M_0 e^{\frac{-t}{T2*}}$ [1]

2.3.3 Relaxation in an inhomogeneous $\mathbf{B_0}$ field (T2*)

If the $\mathbf{B_0}$ of the magnet was reasonably homogeneous, the FID would be an exponential decrease with T2 as time constant. In reality, $\mathbf{B_0}$ is heterogeneous because of local microscopic and macroscopic effects. Spins lose phase coherence and thus $\mathbf{M_{xy}}$ decreases faster. The FID signal decays with a time constant $T2* < T2$ (figure 2.6).

Chapter 3

Magnetic Resonance Imaging (MRI)

In MRI, the signal of hydrogen is usually used to collect information on the spatial distribution of molecules (often water) in a sample. MRI provides informations on morphology and on physiology. It's a non-invasive imaging method which allows a view of the subject in slices or 3D [4].

3.1 Signal localization and image reconstruction

Spatial localization of the NMR signal is needed to create images. To do this, spatially linear fields created by gradient coils are added to the static field $\mathbf{B_0}$, usually in three orthogonal directions. We refer here to x,y,z but in practice axes are interchangeable and can be combined to allow imaging in any oblique plane. In a volume, a slice is first selected by a slice-selection gradient G_{ss} applied in z-direction. For different slice orientations (coronal, sagittal, axial), G_{ss} is applied along a different axis (figure 3.1). Then within this slice, the selection in the x-direction is done by a frequency-encoding gradient G_ω and in the y-direction by a phase-encoding gradient G_ϕ.

Without applied gradients, spins have ω_0 as frequency, and can undergo the 90 degree excitation if the frequency ω_p of the pulse (B_1) is equal to ω_0. As described before in section 2.2 the frequency is linked to the magnetic field, so if a gradient of magnetic field is applied along a certain direction, spins would have a different frequency depending on their position in this direction. This is the role of the slice-selection gradient. G_{ss} is applied during the excitation, and so only spins which have a frequency that lies within the bandwidth of the pulse are excited. Only the excited spins can create signal, and thus a slice localized in the z-direction is selected. The slice thickness depends on the strength of the gradient and on the frequency band selected. The stronger the gradient, the thinner the slice. The wider the frequency band, the wider the slice.

To create a 2D image within the excited slice we add two more gradients, G_ω in the x-direction and G_ϕ in the y-direction:

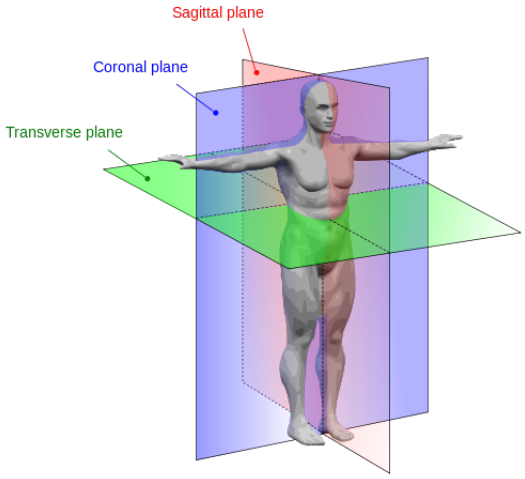

Figure 3.1: Anatomical planes in a human

1. In the x-direction the frequency-encoding or readout gradient is added. That means spins would have a different frequency depending on their position in the x-direction. As the difference in frequency disappears if the gradient is stopped, the signal is acquired while this gradient is applied.

2. In the y-direction the phase-encoding is added. Thus spins would have a different frequency depending on their position in the y-direction. When this gradient is turned off, meaning that there are no longer any differences in frequency, the accumulated phase differences persist. The phase of spins ϕ depends on their frequency ω but also on the time interval δt, $\phi = \omega * \delta t$, thus if gradients of different time interval or different amplitude are applied, spins can be localized on the y-direction.

To summarize the cycle, the excitation pulse and G_{ss} are applied at the same time so a slice of the sample is selected, then G_ϕ is used and finally G_ω during the acquisition. Data are extracted by a Fourier Transform and thus one line of the Fourier space is obtained. Then to get other lines of the Fourier space, the same cycle is used but G_ϕ is applied with a different amplitude. Finally, another Fourier Transform is done to create the image in the real space. To select another slice, the frequency of the pulse is changed and the cycle is run again and G_ϕ changed for each line.

The acquisition time (T_{ac}) is the time needed to create an image and it determines the length of the MRI sequence:

$$T_{ac} = TR * N_p * N_{ex} \tag{3.1}$$

With TR : time for each line

N_p: number of lines

N_{ex}: number of averages (if N_{ex} increases, the quality of the image does too)

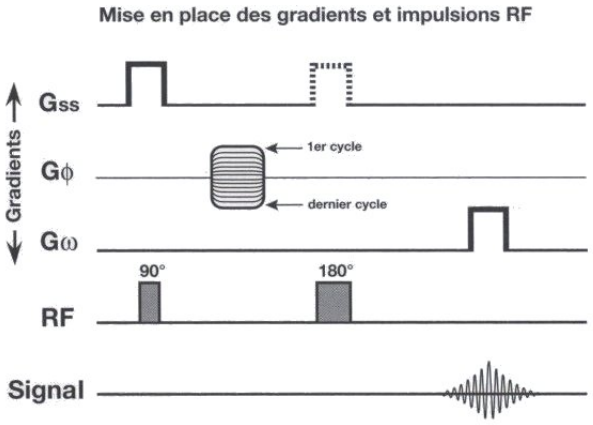

Figure 3.2: Basic spin-echo imaging [1]

The field of view (FOV) represents actual in-plane dimensions of the slice. The matrix size defines the numbers of rows and columns. A volume element (voxel) is the basic volume of the sample which signal intensity is reported on a picture element (pixel). The dimensions of the FOV and the size of the matrix determine the spatial resolution (size of a pixel). With a fixed FOV, as the size of the matrix increases, the size of the pixel decreases.

3.2 MRI sequences

3.2.1 Basic spin-echo imaging

The FID signal, because of the heterogeneities in $\mathbf{B_0}$, has T2* as time constant instead of T2. Basic spin-echo imaging (figure 3.2) is used to acquire a signal with T2 as time constant and to avoid loss of signal. In this sequence, a 180 degree RF excitation is done after the 90-degree RF excitation to have spins with identical phase. Following the 90 degree pulse, spins dephase due to molecular heterogeneities (figure 3.3). The 180 degree pulse is done at $t = \frac{TE}{2}$ after the excitation. This second excitation reverses the net dephasing without changing the direction of rotation. Spins at a higher frequency had advanced relative to lower frequency spins, so after the 180 degree excitation this order would be inverted. Following a second period of $\frac{TE}{2}$ the dephasing has been cancelled out and the spins are in phase. A spin-echo signal is received at t=TE. Basic spin-echo imaging is often used in imaging but has a long acquisition time due to the requirement that TR is long enough to allow signal regrowth following the 90 degree excitation [1].

TE= Echo Time, time between RF excitation and the acquisition.

TR= Repetition Time, time between two 90 degree RF impulsions= time of the regrowth of $\mathbf{M_z}$ = time between two rows of the matrix.

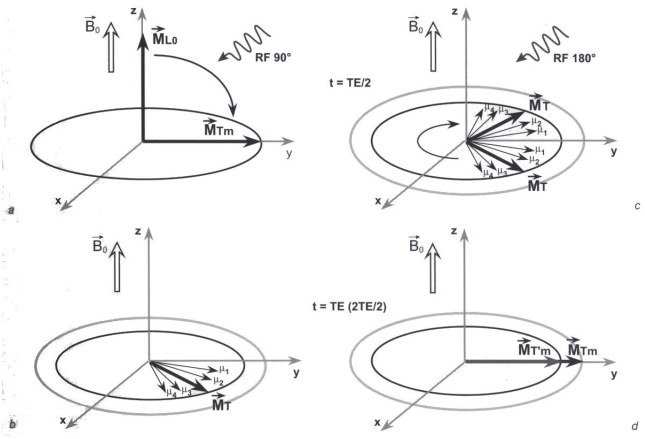

Figure 3.3: Phasing of spins due to 180 degree excitation [1]

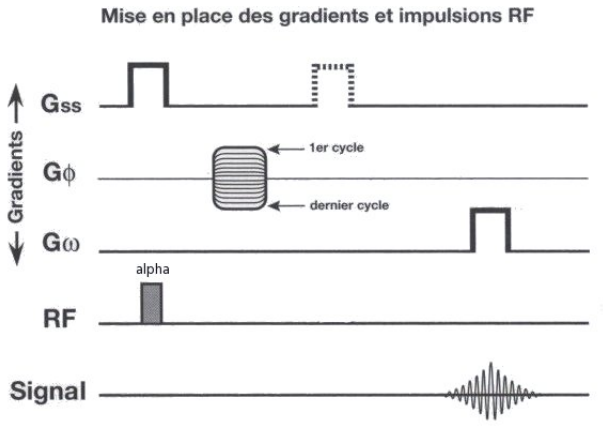

Figure 3.4: Basic gradient-echo imaging [1]

The NMR signal equation is:

$$S_{se} = \rho \left(1 - e^{\frac{-TR}{T1}}\right) e^{\frac{-TE}{T2}} \tag{3.2}$$

S_{se} : signal of a spin-echo

ρ : proton density

3.2.2 Basic gradient-echo imaging

These sequences can be shorter because the acquisition can be done just after the excitation. The FLASH sequence (Fast Low Angle Shot) [5] is a special gradient-echo sequence in which the flip angle α is decreased thus TR can be decreased as well (figure 3.4). An optimal flip angle, for SNR and for a given T1, can be chosen according to the theory of the Ernst angle: $\alpha = arccos\left(e^{\frac{-TR}{T1}}\right)$. The acquisition time depends on TR and hence the ability to decrease TR means that gradient-echo acquisitions are usually shorter than spin-echo acquisitions.

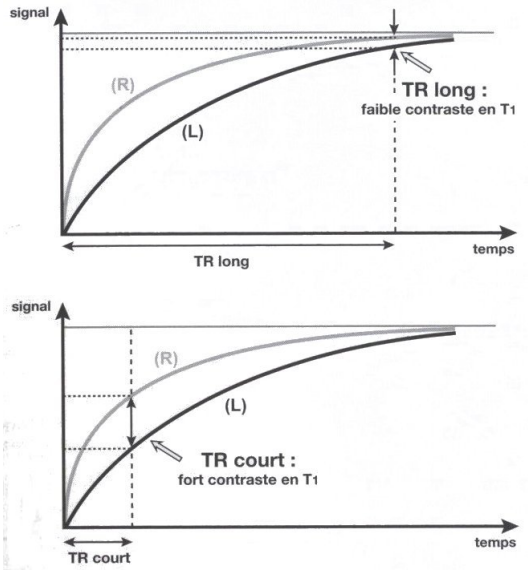

Figure 3.5: TR controls the T1 contrast [1]

3.3 Proton density-weighting and T1, T2 contrast

The contrast between the signals of tissue comes from their differences in T1, T2, density of protons and importantly from parameters of the sequence. More sophisticated sequences, not described here, can include diffusion, flow and other contrast mechanisms. The contrast is then translated into pixel values in the final image. TE and TR parameters can dominate the signal [1].

3.3.1 Influence of TR: T1-weighted image

TR determines the level of the regrowth of $\mathbf{M_z}$ linked to the T1 of tissue, and so can determine the T1 contrast, in which case T1-weighting is obtained. If $TR > 5 * T1$, $M_z = M_{z0}$ at the end of each cycle. For a shorter TR, the regrowth of $\mathbf{M_z}$ is interrupted. If we have two tissues with a different T1, the first tissue (R) with a short T1 and the second (L) with a long one, they can be distinguished depending on the TR chosen (figure 3.5). For a long TR, M_z of each tissue is equal to M_{z0} so they cannot be distinguished by their T1. For a short TR, $\mathbf{M_z}$ of R regrows quicker than that of L so the signal of R is stronger than the signal of L. The difference in signal level is translated into the value of a picture element (pixel) of the resulting image, and so contrast is observed between L and R. The more we shorten TR, the more T1-weighting we have. TE has to be short to minimize the T2-weighting (section 3.3.2). High signal corresponds to a tissue with a short T1.

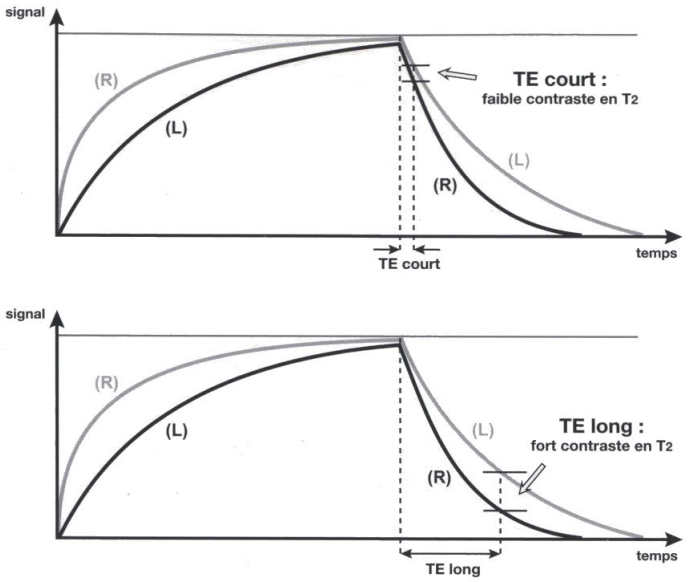

Figure 3.6: TE controls the T2 contrast [1]

3.3.2 Influence of TE: T2-weighted image

TE determines the moment when the signal is measured while the signal decreases. Consider two tissues with different T2: R with a short T2 and L with a long T2. We keep TR long to minimize the T1 contrast. For a too short TE, differences in speeds of decrease are not noticeable and the tissues cannot be distinguished by their T2. But if TE is long enough, we can see that the signal of L is stronger and decreases more slowly (figure 3.6). The difference in signal level is translated into the value of pixel of the resulting image, and so contrast is observed between L and R. The more we lengthen TE, the more the sequence is T2-weighted up to a limit of the decay of the signal below noise. A high signal corresponds to a tissue with a long T2. The acquisition time is long as the TR is long.

3.3.3 Proton density-weighted image

In a proton density weighting, TR is long to minimize T1 contrast and TE is short to minimize T2 contrast. Mz0 is proportional to the density of proton so the signal is different depending on the density of water in tissues. The contrast is weak because biological tissues have little differences in water density (figure 3.7).

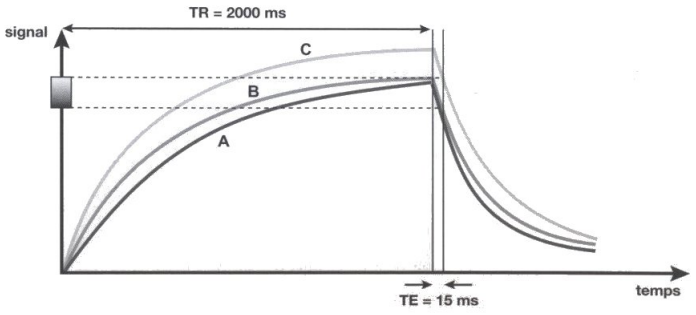

Figure 3.7: Parameters for a proton density-weighted image [1]

Chapter 4

MR scanner and field correction

4.1 MR scanner

An MR scanner is composed of four main hardware components: a main magnet, a magnetic field gradient system, an RF system and control electronics (figure 4.1). The main magnet can be a resistive, permanent or superconducting magnet; it generates $\mathbf{B_0}$ field. Superconducting magnets are used for generating higher field strengths than approximately 0.5T and are generally cooled down by liquid helium (4 K). The $\mathbf{B_1}$ field is generated by a transmitting antenna and the signal is acquired by a receiving antenna. A single antenna can be used for both excitation and reception, and is then referred to as a transceiving antenna [4].

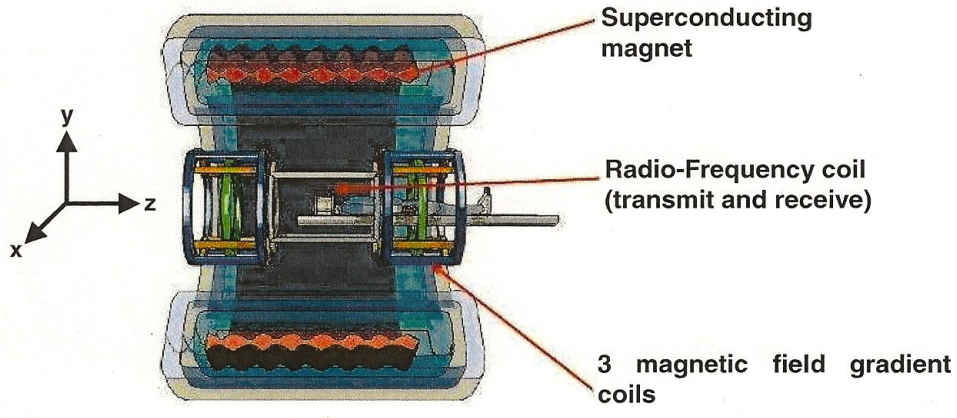

Figure 4.1: MR scanner

4.2 Shimming

In reality, $\mathbf{B_0}$ is never perfectly homogeneous. Inhomogeneities are caused by tolerances in manufacturing and the magnetic properties of the patient. These variations in the main field can affect the quality of images and thus corrections of $\mathbf{B_0}$ are done by shim systems. The shims can be passive, made of several movable metallic pieces, or active using coils located between the main magnet and the gradients. Some systems use a set of superconducting shims within the magnet to establish the main system homogeneity. To appropriately set the current through the active shim coils, the static field is measured and then corrected by changing the shim coil currents. This process is often applied iteratively until the desired homogeneity has been reached. When a subject (sample or patient) is added in the MR scanner, the magnetic susceptibility of tissue causes additional variations in the magnetic field so 2nd and higher order shims – depending on the system – are adjusted. First order shimming is also used, but the gradient coils are used for this purpose.

Chapter 5

Spherical harmonics

Spherical harmonics can describe the spatial distribution of the magnetic field in a source free region [6]. To understand why spherical harmonics can be used, we start with Maxwell-Ampere's equation:

$$\nabla \times \mathbf{B} = \mu_0 \mathbf{J} + \frac{1}{c^2}\frac{\partial}{\partial t}\mathbf{E}. \tag{5.1}$$

If we consider only static fields then we have $\frac{\partial}{\partial t}\mathbf{E} = 0$ and equation 5.1 becomes:

$$\nabla \times \mathbf{B} = \mu_0 \mathbf{J}. \tag{5.2}$$

In a region of interest inside the antenna and around the phantom, the current density $\mathbf{J}$ and the source charge ρ are zero and thus equation 5.2 is now:

$$\nabla \times B = 0. \tag{5.3}$$

If we take the curl of equation 5.3: $\nabla \times \nabla \times B = \nabla(\nabla \cdot B) - \nabla^2 B$ but we have $\nabla \cdot B = 0$ from the Maxwell Gauss equation and we also have $\nabla \times B = 0$, so that from equation 5.3 we find $\nabla^2 B = 0$ which means that each Cartesian component of B obeys Laplace's equation. The total field in z-direction can be written as a sum of spherical harmonics:

$$B_z = \sum_{m=0}^{\infty}\sum_{n=m}^{\infty}(B_{za,n,m}T_{n,m} + B_{zb,n,m}T^{'}_{n,m}) \tag{5.4}$$

where $B_{za,n,m}$ and $B_{zb,n,m}$ [1] are the spherical harmonic coefficients of B_z.

The spherical harmonics are:

$$T_{n,m} = r^n P_{n,m}(cos(\theta))cos(m\phi) \tag{5.5}$$

[1] The units of $B_{za,n,m}$ and $B_{zb,n,m}$ are $\mu T/m^n$ where n is the order of the harmonic. From figure 5.1 we see that to have B_z in μT, coefficients need to have a different unit depending on the order of the harmonic because the order changes the units of the harmonic.

n	m	$T_{n,m}$	$T'_{n,m}$
0	0	1	0
1	0	z	0
1	1	x	y
2	0	$\left(2z^2 - y^2 - x^2\right)/2$	0
2	1	$3xz$	$3yz$
2	2	$3\left(x^2 - y^2\right)$	$6xy$
3	0	$z^3 - 3z\left(x^2 + y^2\right)/2$	0
3	1	$\left(12xz^2 - 3xy^2 - 3x^3\right)/2$	$\left(12yz^2 - 3x^2y - 3y^3\right)/2$
3	2	$(15x^2 - 15y^2)z$	$30xyz$
3	3	$15x^3 - 45xy^2$	$-15y^3 + 45yx^2$

Table 1: Table of Spherical Harmonics in Cartesian Coordinates

Figure 5.1: Spherical harmonics

and

$$T^{'}_{n,m} = r^n P_{n,m}(cos(\theta))sin(m\phi) \tag{5.6}$$

with (r,θ,ϕ) as standard spherical coordinates and where $P_{n,m}$ are Legendre polynomials

$$P_{n,m}(x) = \frac{(1-x^2)^{\frac{m}{2}}}{(-1)^n 2^n n!}\frac{d^m}{dx^m}\frac{d^n}{dx^n}\left[(1-x^2)^n\right]. \tag{5.7}$$

The complexity of the spherical harmonics increases with the harmonic order (n) and degree (m). The first few spherical harmonics are simply a uniform field followed by x, y and z gradients which are followed by harmonics with more complex spatial patterns. The main field of the magnet is proportional to $T_{0,0} = 1$, the gradient coils produce fields proportional to $T_{1,0} = z$, $T_{1,1} = x$ and $T^{'}_{1,1} = y$ and each shim coil is designed to produce a single spherical harmonic that compensates the heterogeneities of the magnetic field.

Chapter 6

Implementation of B_0 shimming with ferromagnetic ink

Working at UHF is an interest for researchers because if the magnetic field is higher, then the magnetization is higher too and the SNR is increased (chapter 2). But unfortunately, when the main field increases, heterogeneities due to susceptibility differences become more significant. The magnetization in a material is related to the magnetic field by: $\mathbf{M} = \frac{\chi_m}{\mu_0(1+\chi_m)}\mathbf{B}$ where $\mathbf{B}$ is $\mathbf{B_0}$, χ_m is the magnetic susceptibility of a material and μ_0 is the vacuum permeability. Moreover the total magnetic field in a region is the sum of the field created by the magnet and the magnetization of the body. Since the magnetic field in the body varies depending on the magnetic susceptibility of the tissue [6], this variation increases with B_0. For most studies using a clinical MR scanner ($\leq 3T$), these heterogeneities are reasonably corrected by shim coils but with a 7T MR scanner such as is used in research at NeuroSpin, a higher order shim is preferable. Standard sets of shim coils are only able to correct second or third order field heterogeneities because the number of shim coils is limited by the space they take in the magnet bore. Shim coils may also interact with the gradient coils to produce spatially and temporally complex eddy currents that take a long time to decay. To achieve higher order shimming without taking excessive bore space or producing extra eddy currents one can make ferromagnetic shims by printing copier toner on paper and placing the result around the antenna [7] [8]. The idea is to first acquire a map of B_0 with the scanner, then to determine with a Spherical Harmonic Transform [9] [10] the spherical harmonics and their magnitude. Finally, suitable ferromagnetic shims (ferroshims) would be applied to correct the inhomogeneities and allow an improved image of the brain.

6.1 Producing the Ferroshims

For this study two programs, written in Python, were needed:

1. The purpose of the first program is to calculate the distribution and amount of magnetization needed to produce one or more given spherical harmonics. The distribution of magnetization is done on the surface of a cylinder as the paper will be put around the antenna and depends on the size of this antenna. The output of this program is a vector – a list of values corresponding to positions – of amount of ink .

2. The second program creates a postscript program to convert the vector of amount of ink into a matrix and then to print the matrix of ink on six A4 pieces of paper to cover the outer surface of the antenna.

My job was to write the second program and to improve some parts of the first one such as the ease of changing input parameters and the reading of output parameters. I also performed the experiments and analyzed the data.

6.1.1 Spherical harmonic creation

Let us see more precisely how the first program works. The magnetization scalar potential produced by a limited amount of magnetization is [[11], p196]:

$$d\Phi = -\frac{\mathbf{m}}{4\pi}\nabla\left(\frac{1}{v}\right)dA \tag{6.1}$$

and

$$\frac{1}{v} = \frac{1}{f}\sum_{n,m}^{\infty}\epsilon_m\frac{(n-m)!}{(n+m)!}P_{n,m}(cos(\alpha))\left(\frac{1}{f}\right)^n[cos(m\psi)T_{n,m} + sin(m\psi)T^{'}_{n,m}][[12], p887] \tag{6.2}$$

where $m\ dA$ is the magnetization created by an element of ink of area dA, (f,α,ψ) are the spherical coordinates of the source point – that is the coordinates of the magnetization – and (r,θ,ϕ) are the coordinates of the field point. $P_{n,m}$, $T_{n,m}$, $T^{'}_{n,m}$ are defined in chapter 5 and ϵ_m is the Neumann factor:

$$\epsilon_m = 2 - \delta_{0,m} = \begin{array}{c|l} 1 & m = 0 \\ 2 & m \neq 0 \end{array} \tag{6.3}$$

In our case, the magnetization is in the z-direction so equation 6.1 becomes:

$$d\Phi = -\frac{m_z}{4\pi}\frac{\partial}{\partial z}\left(\frac{1}{v}\right)dA. \tag{6.4}$$

If we use $\frac{1}{v}$ from equation 6.2 in equation 6.4 and apply the z-derivatives of spherical harmonics [6]:

$$\frac{\partial T_{n,m}}{\partial z} = (n+m)T_{n-1,m} \quad \frac{\partial T^{'}_{n,m}}{\partial z} = (n+m)T^{'}_{n-1,m} \tag{6.5}$$

then we have:

$$d\Phi = -\frac{m_z}{4\pi}\left[\sum_{n,m}^{\infty}\epsilon_m\frac{(n-m)!}{(n+m-1)!}P_{n,m}(cos(\alpha))\frac{1}{f^{n+1}}[cos(m\psi)T_{n-1,m} + sin(m\psi)T^{'}_{n-1,m}]\right]dA. \tag{6.6}$$

According to [[6], chapter 4, p68], the scalar potential should be in the form $T_{n+1,m}$ to correspond to the magnetic field. Thus n is replaced by n+2 such that:

$$d\Phi_{n,m} = -m_z \frac{\epsilon_m}{4\pi} \frac{(n-m+2)!}{(n+m+1)!(n+m)!} P_{n+2,m}(cos(\alpha)) \frac{1}{f^{n+3}} [cos(m\psi) T_{n+1,m} + sin(m\psi) T'_{n+1,m}] dA \quad (6.7)$$

and so we obtain the coefficients of the magnetic field's spherical harmonics produced by a small amount of magnetization m_z at a point (f,α,ψ):

$$dB_{za,n,m} = -m_z \frac{\epsilon_m}{4\pi} \frac{(n-m+2)!}{(n+m)!} P_{n+2,m}(cos(\alpha)) \frac{1}{f^{n+3}} cos(m\psi) dA \quad (6.8)$$

$$dB_{zb,n,m} = -m_z \frac{\epsilon_m}{4\pi} \frac{(n-m+2)!}{(n+m)!} P_{n+2,m}(cos(\alpha)) \frac{1}{f^{n+3}} sin(m\psi) dA \quad (6.9)$$

The total value of these coefficients is the sum of the contribution from each patch of magnetization. Thus we have a list of desired magnetic field coefficients and a list of unknown magnetization values. The problem is to find magnetization values which produce the desired field such that the total magnetization is minimized.

6.1.2 Linear Programming

Problems of this sort can be solved using linear programming which has been implemented in the Python library PuLP [13]. Linear programming (LP) [14] is a mathematical optimization method to achieve the best result (a value that needs to be maximized or minimized). LP can optimize a linear objective function P(x) which is a real-valued affine function subject to linear equality and linear inequality constraints, such as $x \geq 0$ and $A*x = b$. A is a matrix and b a column vector. The objective function to be minimized in our problem is the total magnetization which is constrained by the equation $B = S * M$ where B is the vector of spherical harmonic coefficients for the magnetic field, M is the vector of magnetization but we only know the position of each magnetization and not the values, and S is the matrix that links B and M according to equation 6.8 and 6.9. Linear programming solves the problem minimizing the total amount of ink. The program produces a solution which is a vector of amount of ink.

6.1.3 Printing the matrix

The basic plan is to identify (x,y) coordinates on a flat sheet that correspond to the (f,α,ψ) coordinates that the ink patches – uniformly shaped rectangles covering the surface of the antenna– will take after the paper is wrapped around the cylindrical antenna. The size of the patches are determined by the size of the antenna and the number of segmentations of the antenna's surface. Then these patches are assigned a grey level that corresponds to the amount of ink. The need to form a shim from six connected pieces of paper complicates the design process. Finally, the python program creates a postscript file that allows us to print the ink matrix.

6.2 Testing the Ferroshims

6.2.1 Materials

This part of the study was performed on a Siemens Magnetom 7T MRI (Siemens Medical Systems, Erlangen) with a AC84 Head Gradient coil capable of 80 mT/m, slew rate of 333mT/m/s and a Circularly Polarized (CP) Birdcage coil. The system software version was VB15. The phantom was a spherical bottle of silicone oil. An initial experiment was done using a Canon C2030i printer but the ink was not ferromagnetic, thus the final printer used was a HP 3005x Q7816A with HP LaserJet 51 cartridge.

6.2.2 Experiments

Although we eventually wish to produce higher order harmonics, we start using harmonics that can be produced by the shim coils since the siemens scanner can calculate them. This way we can check if our ferroshims are working properly.
The goal of the first experiment is qualitative, and is to determine if the targeted spherical harmonic is actually produced.
Three ferroshim matrix patterns were printed:

1. One ferroshim designed to produce the spherical harmonic $T_{2,0}$ with a magnitude $B_{za,2,0} = 5\mu T/m^2$.
2. Another ferroshim to produce $T_{2,2}$ with a magnitude of $B_{za,2,2} = 3\mu T/m^2$.
3. A further ferroshim producing both $T_{2,0}$ and $T_{2,2}$.

The second experiment is quantitative, its goal is to check if the spherical harmonics generated by the ferroshims generate a change proportional to the magnitude(s) they were designed to produce. We also designed ferroshims to produce either positive or negative harmonic magnitudes to check that both are possible. For a future experiment with an animal or a human, the magnitude of spherical harmonics to be generated by the ink will be deduced from a B_0 map and a ferroshim will be designed to produce a homogeneous field.

Four matrix patterns were printed (see appendix: Ink Matrices):

1. Two matrices to produce the spherical harmonic $T_{2,0}$, one for a positive magnitude $B_{za,2,0} = 2\mu T/m^2$ and the other for a negative magnitude $B_{za,2,0} = -2\mu T/m^2$.
2. Two others to produce $T_{2,2}$ and again positive and negative magnitudes.

First the phantom was placed on the MRI and a map of the static field was calculated [1] without the ink. The phantom and the antenna were removed and replaced in the same position five times and

[1] Maps are calculated using the scanner routine 3D Shim

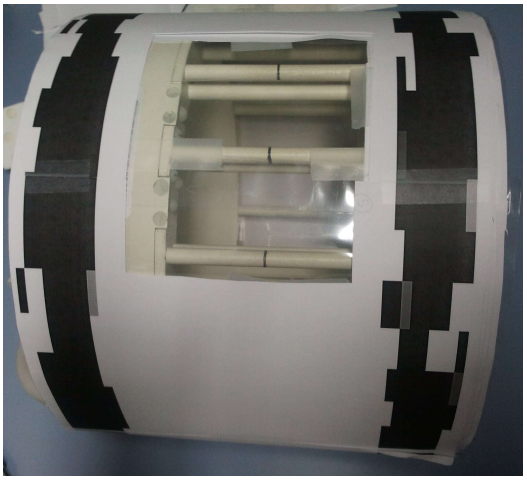

Figure 6.1: Sheet of paper with ferromagnetic ink around the antenna

the B_0 map was acquired to determine the average offset of spherical harmonic without ferroshim. Then sheets were fixed one by one around the antenna (figure 6.1) and then five times again the phantom, the antenna and sheets were placed in the same position and the B_0 map was acquired. The removal and replacement of the phantom and the antenna was needed to prove that the field is really modified by the ink and not by the repositioning of the apparatus. It is also a method to reproduce a future experiment on a human who would be moved when the sheets would be added. Additionally, several acquisitions allows us to calculate the variability.

6.3 Results

6.3.1 First experiment

The results from the first experiment are shown in figure 6.2. The x-axis of this plot shows all the coefficients $B_{za,n,m}$ and $B_{zb,n,m}$ of the spherical harmonics $T_{1,0}$, $T_{1,1}$, $T_{2,0}$, $T_{2,1}$ and $T_{2,2}$. $B_{za,n,m}$ corresponds to $A_{n,m}$ and $B_{zb,n,m}$ to $B_{n,m}$. The coefficients equal to zero are not presented. The y-axis shows the magnitude of these coefficients. Each bar corresponds to a spherical harmonic magnitude acquired from a shim experiment: first from a shim designed to produce $T_{2,0}$ ($T_{2,0}$ ferroshim) with one layer of paper and then with four layers of paper, a $T_{2,2}$ ferroshim with one and then four layers of parker and finally a $T_{2,0} + T_{2,2}$ ferroshim with only one layer of paper. The value of each coefficient shown in the first plot is the spherical harmonic magnitude with its initial offset subtracted so that we can see directly any effect of the applied ferroshim.

First looking at $T_{2,0}$ with one layer of paper, we see that $A_{2,0}$ has a significant value $37 + / - 3\mu T$ compared to the other coefficients and its variation. Then taking $T_{2,0}$ with four layers we see that this

value is much bigger, $A_{2,0} = 131 + / - 3\mu T$. The effect is increased but not multiplied by four. We can thus say that $T_{2,0}$ has been produced by the ink matrix. If we look at $T_{2,2}$ with one layer, we notice that $A_{2,0}$ is increased to $10 + / - 4\mu T$ and $A_{2,2}$ is increased to $19 + / - 3\mu T$. Then looking at $T_{2,2}$ with four layers of paper, $A_{2,0}$ has a lower change than the error bar whereas $A_{2,2}$ is now equal to $67 + / - 3\mu T$ which is not four times the value with one layer. So in this case $T_{2,2}$ is not the only harmonic produced by the ink matrix, $T_{2,0}$ is also created. Paying attention to the results from the shim designed to produce $T_{2,0} + T_{2,2}$, we notice that $A_{2,0} = 101 + / - 4\mu T$ and $A_{2,2} = 7 + / - 4\mu T$, this is a bigger variation than for other coefficients but not equal to previous values with $T_{2,0}$ or $T_{2,2}$ only. Here we have effectively produced both harmonics but they are not as strong as before.

The reason why we do not have a pure $T_{2,2}$ harmonic is possibly due to the sheets of papers having been shifted along the z-axis which means that according to equation 5.5 and 5.6 when the spherical coordinate θ changes, we have a different set of harmonics. That is also possibly the same reason that there is only a small variation with $T_{2,0} + T_{2,2}$. Another reason for not having pure harmonics is that our defined patches are too big while these patches should be very small according to the equation 6.8 and 6.9 we used in our program. Another problem is that when we add more layers, the spherical coordinate r from the isocenter of the antenna increases and sheets are not enough long to fit the new circumference of the antenna, so the matrix is shifted and thus the value of a coefficient is not exactly multiplied by four when we stack up four paper layers. Finally, we cannot compare values produced by the $T_{2,0}$ ferroshim to those of $T_{2,2}$ ferroshim because the magnitude of spherical harmonics they were designed to produce were not the same. The priority was to check if the correct harmonics were produced not to search for harmonic magnitudes for which the optimization program would produce a valid result.

6.3.2 Second experiment

Now, let us examine the result from the quantitative experiment with the graph 6.3. The x-axis and the y-axis are the same as the ones on the previous plot. But here we have bars corresponding to a $T_{2,0}$ ferroshim with a positive magnitude, a $T_{2,0}$ ferroshim with a negative magnitude, and then a $T_{2,2}$ ferroshim with a positive magnitude. As the changes were not significant enough compared to changes with other ferroshims, we used six layers of the $T_{2,2}$ ferroshim with a positive magnitude and six layers of the $T_{2,2}$ ferroshim with a negative magnitude. The offsets have been subtracted as before.

Looking at $T_{2,0}$, we notice that only the value of $A_{2,0}$ has changed and that for both positive and negative $T_{2,0}$, $|A_{2,0}| = 49 + / - 4\mu T$. That means we have a constant change in the coefficient of spherical harmonic whether the magnitude of the spherical harmonic produced is negative or positive. But the magnitude produced is not the same as the one expected, it should be $A_{2,0} = 2\mu T$ (section 6.2.2), which can be explained by the existence of an unknown calibration constant depending on magnetic properties of the ink . Then if we look at the $T_{2,2}$ ferroshim with six sheets, both $B_{2,1}$ and $A_{2,2}$ are created. For the positive

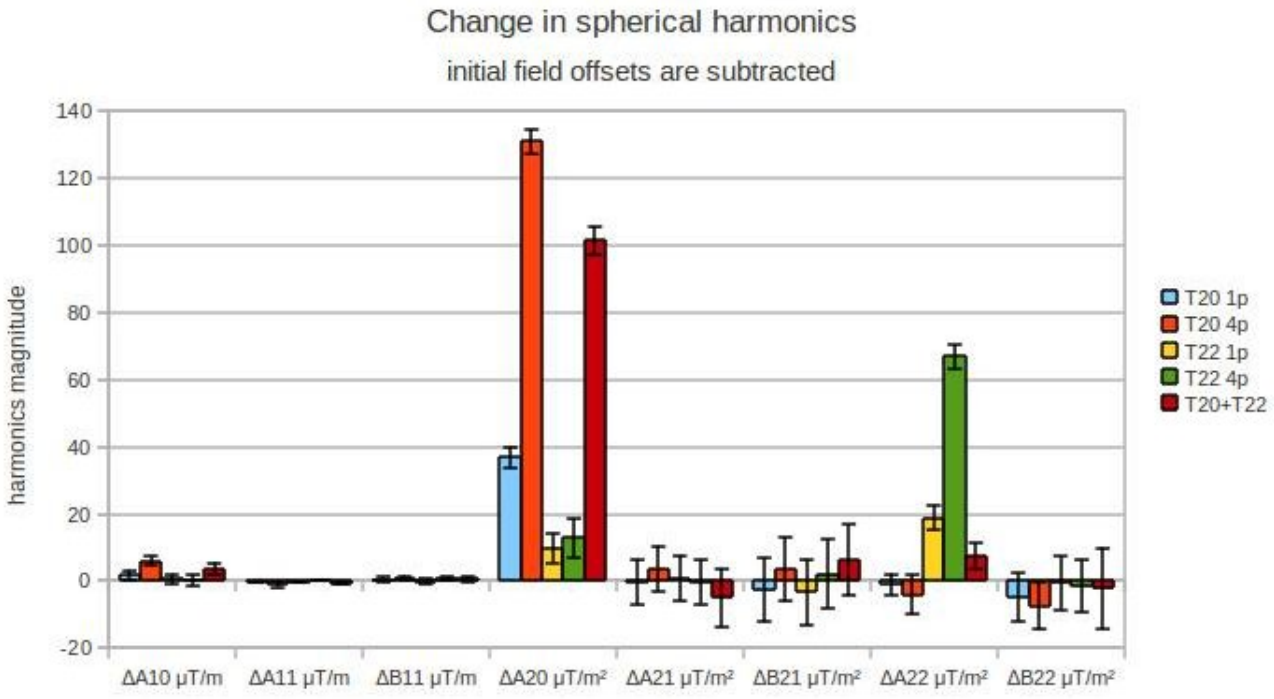

Figure 6.2: Results from the first experiment

$T_{2,2}$ ferroshim, $B_{2,1} = 9 +/- 6\mu T$ and $A_{2,2} = 13 +/- 11\mu T$, for the negative $T_{2,2}$, $B_{2,1} = 11 +/- 5\mu T$ and $A_{2,2} = -37 +/- 3\mu T$. The possible causes for harmonic impurity are probably the same as with the first experiment. However in this second experiment we know that the shims were slightly shifted along the z-axis by approximately 0.5 cm. This is because plastic pockets were constructed to hold the shims on the antenna so that scotch tape was not necessary. Unfortunately the recalculated page margins did not perfectly center the ferroshims in this second experiment. Note that, for the $T_{2,2}$ ferroshim experiments, the rise in $\Delta B_{2,1}$ passes its error bound and the drop in $\Delta A_{2,2}$ may be caused by this shift along z.

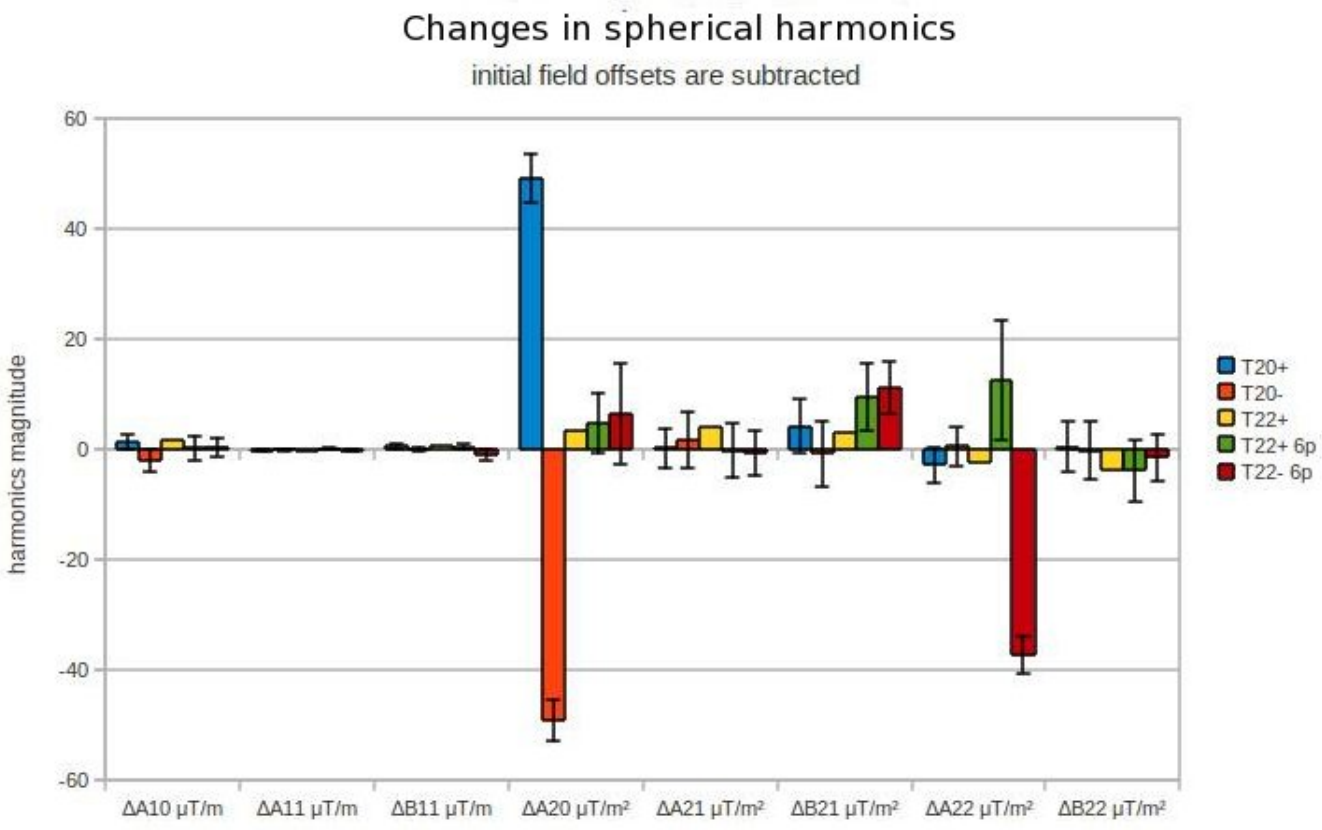

Figure 6.3: Results from the second experiment

Chapter 7

Conclusion and future work

We can say that we are able to produce the spherical harmonic $T_{2,0}$ in both positive and negative magnitudes. However, we are having problems producing $T_{2,2}$ as the magnitudes are not as expected. We think this is caused by the size of the patches and the shifting along z. If this is the case, these problems could be fixed by decreasing the patch size, perfectly centering the sheets, and correcting the change in radius caused by the multiple layers. But if these experiments are not successful then simulation work would be require to understand the problems.

When harmonics can be reliably produced, the next step is to map a field and to correct it with a specifically designed ferroshim. This should be done many times to increase confidence, first on a phantom and then on animals and eventually on humans. The ultimate goal is to design a custom ferroshim for every patient in just a few minutes.

Appendix: Ink Matrices

The size of the real matrices is 26 cm wide and 100 cm long.

The T20 ferroshim for a positive magnitude

The T20 ferroshim for a negative magnitude

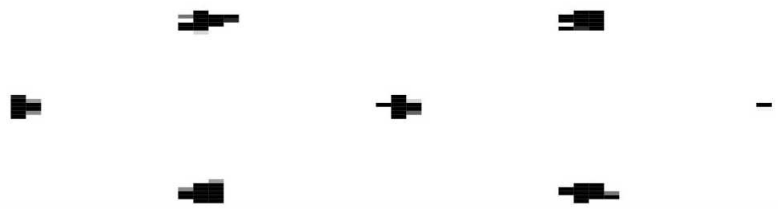

The T22 ferroshim for a positive magnitude

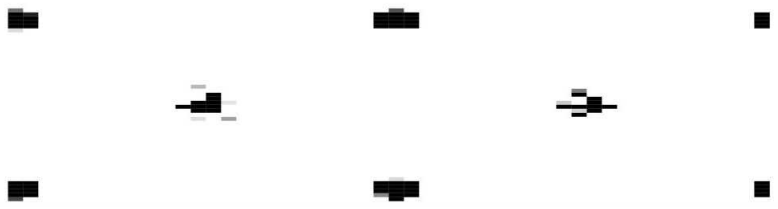

The T22 ferroshim for a negative magnitude

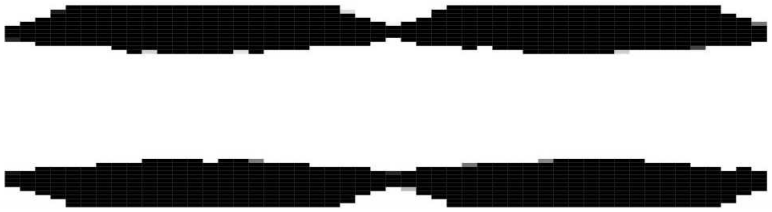

The T20+T22 ferroshim for a positive magnitude

The T20+T22 ferroshim for a negative magnitude

Bibliography

[1] Kastler B and Vetter D. *Comprendre l'IRM, manuel d'auto-apprentissage.* Masson, 6eme edition, 2006.

[2] Jesmanowicz A, Starewicz P, and Hyde J.S. Determination of shims needed for correction of tissue susceptibility effects in fMRI. *Proc.Intl.Soc.Mag.Reson.Med.*, 2000.

[3] Jesmanowicz A, Roopchansingh V, Cox R.W, Starewicz P, Punchard W.F.B, and Hyde J.S. Local ferroshims using office copier toner. *Proc.Intl.Soc.Mag.Reson.Med*, 2001.

[4] Liang Zhi-Pei and Lauterbur Paul, C. *Principles of Magnetic Resonance Imaging: A signal processing perspective.* Wiley-IEEE Press, 1999.

[5] Haase A, Frahm J, Matthaei D, Hnicke W, and Merboldt KD. Flash imaging: rapid NMR imaging using low flip angle pulses. *J Magn Reson. 67(2): 25866.*, 1986.

[6] Edler Karl. *Spherical Harmonic Inductive Detection Coils and their use in Dynamic Pre-emphasis for Magnetic Resonance Imaging.* PhD thesis, Department Of Physics And Astronomy University Of Manitoba Winnipeg, 2010.

[7] Hetherington H.P, Kuznetsov A.M, Avdievich N.I, and Pan J.W. Higher order B0 shimming of the human brain at 7T. *Proc.Intl.Soc.Mag.Reson.Med*, 2009.

[8] Evans C.J, Jezzard P, and Clare S. Shim requirements for high-order localised shimming of the human brain. *Proc.Intl.Soc.Mag.Reson.Med*, 2007.

[9] Healy Jr D, M, Rockmore D, Kostelec P, J, and Moore Sean. FFTs for the 2-sphere – improvements and variations, 1998.

[10] Kostelec Peter, David K. Maslen, Rockmore Daniel, N, and Healy Jr Dennis. Computational harmonic analysis for tensor fields on the two-sphere.

[11] Jackson John, David. *Classical Electrodynamics.* Wiley, Third Edition, 1999.

[12] Morse Philip, M and Feshbach Herman. *Methods of theoretical physics.* McGraw-Hill Book Company Inc., 1953.

[13] Mitchell Stuart, Kean Anita, Mason Andrew, O'Sullivan Michael, and Antony Phillips. Optimization with PuLP, 2009. https://packages.python.org/PuLP/.

[14] Pierre Donald, A. *Optimization Theory with applications.* Dover, 1969.